

# Optimal Estimation of Deterioration from Diagnostic Image Sequence

Dimitry Gorinevsky, *Fellow, IEEE*, Seung-Jean Kim, *Member, IEEE*, Shawn Beard, Stephen Boyd, *Fellow, IEEE*, and Grant Gordon

**Abstract**—This paper considers estimation of pixel-wise monotonic increasing (or decreasing) data from a time series of noisy blurred images. The motivation comes from estimation of mechanical structure damage that accumulates irreversibly over time. We formulate a Maximum A posteriori Probability (MAP) estimation problem and find a solution by direct numerical optimization of a log-likelihood index. Spatial continuity of the damage is modeled using a Markov Random Field (MRF). The MRF prior includes the temporal monotonicity constraints. We tune the MRF prior, using a spatial frequency domain loopshaping technique to achieve a tradeoff between noise rejection and signal restoration properties of the estimate.

The MAP optimization is a large-scale Quadratic Programming (QP) problem that could have more than a million of decision variables and constraints. We describe and implement an efficient interior-point method for solving such optimization problem. The method uses a preconditioned conjugate gradient method to compute the search step. The developed QP solver relies on the special structure of the problem and can solve the problems of this size in a few tens of minutes, on a PC.

The application example in the paper describes structural damage images obtained using a Structural Health Monitoring (SHM) system. The damage signal is distorted by environmental temperature that varies for each acquired image in the series. The solution for the experimental data is demonstrated to provide an excellent estimate of the damage accumulation trend while rejecting the spatial and temporal noise.

**Index Terms**—Optimal estimation, spatio-temporal filtering, regularization, interior-point method, isotonic regression, Markov Random Field.

## I. INTRODUCTION

WE consider a time series of noisy blurred images where the underlying signal is pixel-wise monotonic increasing (or decreasing). The paper describes an optimal estimation approach for such signal. The problem formulation is motivated by estimation of mechanical structure damage from a time series of diagnostic images. The damage accumulates irreversibly over time. The application example in the paper is structural damage estimation using a Structural Health Monitoring (SHM) system. The damage signal is blurred and contains sensor noise and a variation caused by environmental factors.

Development of SHM systems has been attracting much attention recently; see [56], [57], [58] for a representative sample of the work. The main applications of SHM are in

aerospace and civil engineering for automated monitoring of structural integrity for high value assets. In particular, mandatory periodic inspections of aircraft structure could be automated using SHM. The SHM data acquired between aircraft flights or for civil structures are subject to broadly varying environmental conditions, such as temperature. An effective estimate of structural damage must be unaffected by or correctable for environmental conditions. Detection of a defect of ‘significant’ size must be almost entirely free from false alarms and missed faults. This motivates the problem considered herein.

The model for a series of images where underlying monotonic change is distorted by noise and blur might be potentially useful for applications in geophysics (e.g., earthquake prediction, petroleum extraction), in medical imaging (e.g., detecting a growing tumor from a series of images), in environmental sciences (e.g., detecting irreversible changes, such as global warming trends), and others.

Deblurring of noisy images is covered in many textbooks, e.g., [14], [18], [33]. Particularly relevant to this work are the papers [21], [23], where deblurring filters are designed in spatial frequency domain by loopshaping based on formal engineering specifications. In [21], [23], the coefficients of a noncausal 2-D IIR filter are obtained by solving a design problem formulated as a linear program (LP). An extension to spatio-temporal filtering of a series of images (motivated by SHM applications) is considered in [25]. The filter input is a series of noisy blurred images; the output is cleaned images emphasizing the underlying signal and reducing the noise. The 3-D IIR filter design proposed in [25], [26] shapes both the spatial response and the time response of the filter by finding the 2-D spatial operators in the filter as a solution to an LP. We use an LP-based shaping of the spatial regularization operator in this paper as well, but for a completely different filter structure.

Linear spatio-temporal filtering does not take into account the monotonic nature of the damage accumulation. There is substantial earlier work on estimation with monotonicity constraints. This work on ‘isotonic regression’ has been driven by applications in statistics and operations research and is summarized in the books [2], [50]. Most of that work considers univariate data, lesser part considers multivariable data, and none deals with image data.

Monotonicity constraints in signal processing problems were considered in [20], [22], [49], [53], [55]. Maximum A posteriori Probability (MAP) estimation assuming a monotonic walk prior model of the trend leads to Quadratic Programming (QP) problems, which can be efficiently solved. When

D. Gorinevsky, S.-J. Kim, and S. Boyd are with Information Systems Lab, Dept. of Electrical Engineering, Stanford University, Stanford, CA 94305

S. Beard is with Acellent Technologies Inc., Sunnyvale, CA 94085

G. Gordon is with Honeywell Laboratories, Phoenix, AZ 85027

Manuscript received May 10, 2007. This work was in part supported by the NSF Grant ECS-0529426

estimating monotonic signals, the filtering approach based on constrained optimization provides a substantial improvement over standard linear filtering methods. Some applications of optimization-based estimation based on monotonic walk models are discussed in [27], [54]. The source of monotonicity considered there is an irreversible nature of faults in the system.

This paper considers an extension of the earlier monotonic walk models to a series of images monotonic in time. The proposed MAP estimation problem formulation is related to the cited work in monotonic trending. The fundamental difference here is the inclusion of spatial information about the images. Our observation model assumes a finite impulse response (FIR) blur operator. In the prior model, the spatial smoothness of the underlying image is described using a Markov Random Field (MRF) model. The overall MAP problem is formulated as a large scale QP problem with the linear monotonicity constraints, where the decision variables include the series of image estimates.

A number of prior papers formulate image processing problems as QPs and other constrained convex optimization problems, e.g., see [15], [16], [17], [30], [38], [35]. One issue with the prior work in optimization-based image processing is that the solutions do not scale up well. Another issue is that these optimization approaches are problem specific and require manual tweaking. They are not available as packaged software, such as standard QP and LP solvers.

The image processing QP problem considered in this paper can be solved using standard QP solvers, when the total number of variables (i.e., the pixels in the image series) is modest, say, under 10000. (High quality solvers that can directly handle a QP problem of large size include LOQO [60] and MOSEK [42].) Unfortunately, standard solvers do not scale to practical image sizes. In particular the SHM application considered in Section V of this paper has the size (the total number of pixels) of just under a million, well beyond what standard QP solvers can handle.

In this paper we use a specialized interior-point method for solving the QP problems with  $l_1$  regularization penalties and positivity constraints. The method computes the search step using a preconditioned conjugate gradient (PCG) approach. A version of the method is described in more detail in [32]. The method is very efficient for all size problems; it is particularly efficient for very large problems such as the one considered herein. A simple Matlab implementation of the method, discussed in more detail in Section IV, can solve the QP problems with an excess of two million variables and two million constraints. For finite impulse response blurring and regularization operators, the method scales almost linearly in the number of variables (pixels). Extensive numerical comparison shows that the proposed method is far more efficient and scalable than MOSEK for a class of problems in question.

The idea of using truncated Newton methods or PCG methods for image enhancement, deconvolution, and deblurring is not completely new; e.g., see [41]. Truncated Newton methods have been applied to large-scale problems in several other fields, e.g., image restoration [16], support vector machines [36], and logistic regression [37]. The most important is-

sue is to find an effective preconditioner. For a spatially invariant blur operator, fast Fourier transform (FFT) can be applied in approximate inverse preconditioners to produce very efficient PCG schemes [61], [28], [43]. In [16] those PCGs are incorporated in an iterative method for solving total variation minimization problems. Iterative methods are generalized to deblurring problems with general non-quadratic fidelity criteria in [29]. The preconditioners mentioned above cannot be directly applied to our problem. One of this paper contributions is finding an effective preconditioner for the image-processing QP problem in question.

The contributions of this paper can be summarized as follows.

First, we introduce a new type of image processing problems for a time series of images where underlying data are pixel-wise monotonic. Apparently, despite its usefulness, such problem formulation has not been considered earlier.

Second, we propose an approach to MAP optimal estimation for the problem in question. A sparse MRF prior model is used to account for the monotonicity and spatial smoothness of the underlying image. We propose an optimal sparsity-preserving method for tuning the MRF prior such that the MAP solution satisfies engineering specification for noise rejection and estimation error.

Third, we propose an interior-point method for solving the QP problems of the formulated type. A Matlab implementation of the solver on a PC is suitable for practical-size problems.

Finally, we demonstrate the approach in an important aerospace application – structural health monitoring. We describe an experimentally collected set of SHM data subject to temperature variation and demonstrate the formulation, tuning, and solution of the QP-based image processing problem with monotonicity constraints. A superior quality of recovering underlying damage maps from the SHM data is demonstrated.

Figure 1 shows the implementation steps for the proposed optimization-based image estimation approach. The first block shows the data and decision variables in the MAP estimation problem, which is formulated in Section II. The parameters of a sparse MRF prior model are considered as tuning factors. Section III describes a method for tuning the MRF model. The tuning is done off line and is reflected by the second block in Figure 1 diagram. A specialized large scale convex solver discussed in Section IV of the paper is applied on-line to compute the filtered data as a solution to the QP problem and is shown as the next to last block in Figure 1 diagram. Finally, Section V describes an SHM application including the data collection experiments, implementation of the proposed approach through the steps outlined in Figure 1, and image processing results.

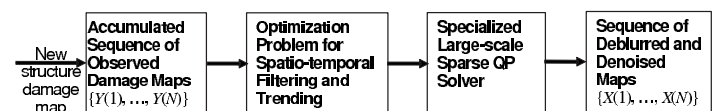


Fig. 1: Optimization-based estimation of damage.

## II. OPTIMIZATION-BASED ESTIMATION PROBLEM

This section introduces a formal mathematical problem statement. Consider an observed data set  $Y$  comprising a sequence of the available diagnostic images. A truth data set  $X$  comprises a sequence of the corresponding underlying damage maps.

$$Y = \{Y(1), \dots, Y(N_t)\}, \quad (1)$$

$$X = \{X(1), \dots, X(N_t)\}, \quad (2)$$

where  $Y(t) \in \mathfrak{R}^{N_1, N_2}$  are the observed damage images and  $X(t) \in \mathfrak{R}^{N_1, N_2}$  are underlying damage images.

The problem is to estimate  $X$  from  $Y$ . An optimal statistical estimate can be obtained by maximizing the conditional probability,  $P(X|Y)$ . In accordance with the Bayes formula, the probability of the hidden underlying data conditional to the observed data can be factorized as

$$P(X|Y) = P(Y|X)P(X)/c, \quad (3)$$

where  $c = P(Y)$  is a constant independent of  $X$ . The MAP (Maximum A posteriori Probability) estimate can be obtained by solving the optimization problem

$$L = -\log P(Y|X) - \log P(X) \rightarrow \min. \quad (4)$$

In order to formulate the optimization-based estimation problem in more detail, we need to define

- the observation model  $P(Y|X)$ , the first factor in (3), and
- the prior probability  $P(X)$ , the second factor in (3).

The observation model and the prior probability are discussed in detail in the subsections to follow. We show that the MAP estimate (4) can be expressed as a QP, a convex constraint optimization problem of the form

$$L = \frac{1}{2} \sum_{t=1}^{N_t} \|Y(t) - B**X(t)\|_F^2 + \frac{1}{2} \sum_{t=1}^{N_t} (X(t), R**X(t)) + \frac{1}{\rho} \sum_{t=2}^{N_t} \|X(t) - X(t-1)\|_1 \rightarrow \min \quad (5)$$

$$\text{subject to } X(t) - X(t-1) \geq 0, \quad t = 2, \dots, N_t \quad (6)$$

where  $(U, V)$  denotes a dot product of the two images  $U$  and  $V$  considered as flat vectors;  $\|U\|_F^2 = (U, U)$ ;  $\|U\|_1$  is the 1-norm (sum of the absolute values of the pixels); and  $R$  is a non-causal 2-D FIR convolution kernel with a maximum tap delay  $M$  and entries  $r_{lm}$ .

The first sum in (5) is the data fit error corresponding to the observation model. The inverse problem of estimating  $X(t)$  from  $Y(t)$  by minimizing the fit error is ill-conditioned. The last two sums in (5) correspond to the prior probability; they add a spatial and a temporal regularization terms. The constraints come from the temporal part of the prior model.

The QP optimization problem (5)–(6) can be solved numerically. Solving the QP problem yields an optimal estimate  $X$ . The solution  $X$  depends on the choice of the spatial regularization operator  $R$  (5). In what follows we consider  $R$  as a tuning parameter and choose it to achieve the desired filtering performance. Section III considers how this can be done.

### A. Observation Model

Consider a probabilistic model for a single diagnostic image at time  $t$ . We assume that the image  $Y(t)$  contains the blurred underlying damage data  $X(t)$  contaminated by noise  $e(t)$ . The observation model has the form

$$Y(t) = B**X(t) + e(t), \quad (7)$$

where  $B$  is a spatially-invariant blur operator expressed by a FIR (finite impulse response) PSF (point spread function) kernel. The notation  $**$  in (7) stands for two-dimensional convolution. Handling of boundary conditions is not considered in detail herein. We assume that one of the standard approaches of image processing analysis is used; see, e.g., [14], [18], [33] for more detail. The noise  $e(t)$  is assumed to be an identically distributed spatially uncorrelated gaussian noise (white noise) with zero mean  $q$ ,  $e(t) \sim N(0, q)$ . In that case the observation probability is

$$P(Y(t)|X(t)) = \frac{1}{Z_t} \exp\left(-\frac{1}{2q} \|Y(t) - B**X(t)\|_F^2\right), \quad (8)$$

where  $\|U\|_F$  is the Frobenius norm of the image array  $U$  (the sum of the squared pixel values) and  $Z_t$  is a scaling constant. The noises  $e(t)$  in (8) are independent for different  $t$ . Thus,  $\log P(Y|X)$  in (4) can be computed by taking a logarithm of (8) and summing up over  $t$ . This yields the first sum in (5).

### B. Spatial MRF model

This and the next two subsections introduce the spatio-temporal prior probability model  $P(X)$  leading to (5)–(6). In this subsection we consider a single time sample  $t$ . Let  $x_{jk} = x_{jk}(t)$  be a pixel of the image  $X = X(t)$ . The indexes  $[j, k]$  define a *lattice point*. We will introduce a neighborhood of a lattice point, a square of the size  $2M + 1$  centered at this point

$$\mathcal{N}_{jk} = \{[l, m] : (|l - j|, |m - k| \leq M, [l, m] \neq [j, k])\}. \quad (9)$$

A MRF probability structure specifies conditional probability for a pixel to be defined by the pixels in the neighborhood (9)

$$P(x_{jk}|X(t) \setminus \{x_{jk}\}) = P(x_{jk}|\{x_{lm} : l, m \in \mathcal{N}_{jk}\}), \quad (10)$$

where  $X(t) \setminus \{x_{jk}\}$  means the entire image  $X(t)$  excluding the pixel  $x_{jk}$ .

Under a positivity constraint assumption (no configuration has a probability equal to zero), the Hammersley-Clifford theorem [5] says that an MRF can be expressed as a Gibbs Field with the probability structure

$$P(X(t)) = \frac{1}{Z} \exp\left(\sum_{c \in \mathcal{C}} -V_c(x_c)\right), \quad (11)$$

where  $\mathcal{C}$  is the set of all cliques (sets of the lattice points that are all neighbors of each other),  $V_c(\cdot)$  are *potential functions*, and  $Z$  is a scaling factor.

Defining the potential functions  $V_c(\cdot)$  allows specifying a consistent MRF model. Following the common practice in image processing, we consider spatially invariant potential functions with the cliques consisting of one or two points. We

use quadratic potential functions, which leads to a Gaussian MRF (GMRF) with the potential

$$\begin{aligned} \sum_{c \in \mathcal{C}} V_c(x_c) &= \sum_{jk} V_{jk} \\ &= \frac{1}{2} \sum_{jk} \left( r_{00} x_{jk}^2 + \sum_{l,m=-M, l,m \neq 0}^M r_{lm} x_{jk} x_{j+l,k+m} \right). \end{aligned} \quad (12)$$

By substituting (12) into (11) and calculating (10), the conditional probability structure can be expressed in the form

$$x_{jk} = r_{00} e_{jk} + \sum_{l,m=-M; l,m \neq 0}^M r_{lm} x_{j+l,k+m} \quad (13)$$

where  $e_{jk}$  are white noise variables. The GMRF model (11), (12) expresses that if a damage is present at a given pixel, there is likely a correlated damage in the neighboring pixels.

The prior model in (11) and (12) can be written in the form.

$$P(X(t)) = \frac{1}{Z_t} \exp \left( -\frac{1}{2} (X(t), R ** X(t)) \right). \quad (14)$$

The necessary and sufficient condition for (14) to represent a valid probability density function is that the 2-D FIR convolution kernel  $R$  is symmetric and positive-definite [34]. Section III considers selection of  $R$  in more detail.

### C. Temporal model

Let us now consider a time evolution of damage at a given spatial location, for a single image pixel. To introduce the model we will temporarily ignore the spatial dependencies and consider a scalar underlying damage signal  $x(t)$ .

Consider a first-order random walk model.

$$x(t+1) = x(t) + \xi(t), \quad (15)$$

where  $\xi(t)$  is i.i.d. (independent identically distributed) noise sequence. To reflect the fact that the damage is accumulating irreversibly, we assume that the noise increments  $\xi(t)$  are always nonnegative, the respective probability distribution is zero for negative argument. Such monotonic damage accumulation model corresponds to the Palmgren-Miner rule used in mechanical damage analysis. Additional discussion and references can be found in [20], [22].

We use an exponential model for the damage accumulation noise  $\xi$  in (15).

$$\xi \sim \begin{cases} e^{-x/\rho}, & x \geq 0 \\ 0, & x < 0. \end{cases} \quad (16)$$

The prior probability can be expressed as a product of the independent probabilities

$$P(X) = \frac{1}{Z_1} \exp \left( -\sum_{t=2}^N V_\xi(x(t) - x(t-1)) \right), \quad (17)$$

where  $V_\xi(x) = -\log p_\xi(x)$ . In accordance with (16),

$$V_\xi(x) = |x/\rho|_+, \quad (18)$$

where  $|x|_+ = x$ , for  $x \geq 0$ , and  $|x|_+ = +\infty$ , for  $x < 0$ .

Consider a scalar observation  $y(t)$  for the same pixel. The observation model (7) can be written as  $y(t) = x(t) + e(t)$ .

By computing the observation model probability  $P(Y|X)$  and substituting the prior model (17) into the MAP problem (4) for the data available over time horizon  $N$  we get

$$\begin{aligned} L &= \sum_{t=1}^N \frac{1}{2q} \|x(t) - y(t)\|^2 + \frac{1}{\rho} \sum_{t=2}^N x(t) \rightarrow \min \quad (19) \\ &\text{subject to } x(t) - x(t-1) \geq 0, \quad (t = 2, \dots, N) \quad (20) \end{aligned}$$

The QP problem (19)–(20) with  $x(t)$  scalar is, equivalent to an isotonic regression problem (see [2], [6], [50]) and can be solved very efficiently, in a linear time. In what follows we consider a generalization of the known problem (19)–(20) for a univariate time series signal to a time series of images.

### D. Optimal estimation problem - spatio-temporal model

We are now ready to introduce a composite spatio-temporal model combining the spatial MRF of Subsection II-B and the monotonic in time damage accumulation model of Subsection II-C. We will formulate the model as a 3-D MRF, causal in time and noncausal in the spatial coordinates.

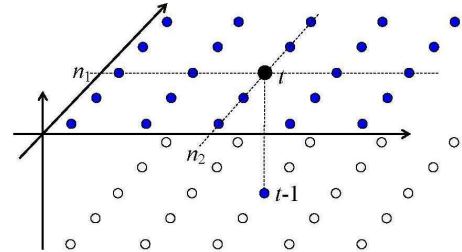


Fig. 2: An example of the neighborhood (21) of a lattice point  $[n_1, n_2, t]$  used in defining the MRF ( $M=2$ ).

The MRF will be defined using the following neighborhoods of the lattice point

$$\begin{aligned} \mathcal{K}_{jk}(t) &= \{[l, m, \tau] : ([l, m] \in \mathcal{N}_{jk} \text{ for } \tau = t, \\ & [l, m] = [j, k] \text{ for } \tau = t - 1, )\} \end{aligned} \quad (21)$$

where  $\mathcal{N}_{jk}$  is as defined in (10). The neighborhood (21) is illustrated in Figure 2. It includes a spatial coordinate square of the size  $2M + 1$  centered at the lattice point and a point shifted back one step in time.

The MRF probability structure assumes that the spatial relation is independent of the temporal relation, so the conditional probabilities are products of spatial and temporal ones. Such separable stochastic models are commonly used in multidimensional signal processing.

We use the following Gibbs Field potential extending and combining (12) and (17):

$$V(X) = \sum_{jk,t=1}^{t=N} V_{jkt} + \frac{1}{\rho} \sum_{jk,t=2}^{t=N} |x_{jk}(t) - x_{jk}(t-1)|_+ \quad (22)$$

$$V_{jkt} = \frac{1}{2} r_{00} x_{jk}(t)^2 + \frac{1}{2} \sum_{l,m=-M}^M \sum_{l,m \neq 0} r_{lm} x_{jk}(t) x_{j+l,k+m}(t) \quad (23)$$

where the notation  $|x|_+$  is the same as in (18). In Figure 2 the neighborhood lattice nodes used in defining the potential (22), (23) are shown as shaded circles.

The prior model (11), (22), (23) can be expressed in the form.

$$P(X) = \frac{1}{Z} \exp \left( -\frac{1}{2} \sum_{t=1}^{N_t} (X(t), R ** X(t)) - \frac{1}{\rho} \sum_{t=2}^{N_t} \|X(t) - X(t-1)\|_1 \right) \quad (24)$$

where we assume that  $X(t) - X(t-1) \geq 0$ ; if that inequality is violated, then  $P(X) = 0$ .

The MAP formulation (4) can be obtained by multiplying the independent probabilities  $P(Y(t)|X(t))$  (8) to yield  $P(X|Y)$  and by substituting  $P(X)$  from (24). The MAP estimate can be expressed through a negative log-likelihood index as in (5)–(6).

### III. LOOPSHAPING TUNING OF THE ESTIMATOR

The filtering properties of a solution to (5)–(6) depend on the regularization operator  $R$ . While other parameters of the problem could be traced back to the problem physics, we consider  $R$  as a free filter design parameter. The operator  $R$  should be set up to ensure an adequate performance of the filter. This section considers how this could be done.

#### A. Tuning requirements

We start by considering the steady state response of the filter. Assume that  $X(t) = X_*$ ,  $Y(t) = Y_*$ , and  $N \gg 1$ . Substituting this into (5)–(6) leads to the steady-state optimization problem

$$\frac{1}{2q} \|Y_* - B ** X_e\|_F^2 + \frac{1}{2} (X_e, R ** X_e) \rightarrow \min. \quad (25)$$

To obtain an optimal estimate  $X_e$  we assume that  $Y_* = B ** X_* + e_*$ , where  $e_*$  is the steady state noise. Substituting this into the unconstrained linear-quadratic problem (25) and solving for  $X_e$  yields

$$X_e = (\mathbf{B}^T \mathbf{B} + \mathbf{R})^{-1} \mathbf{B}^T \mathbf{B} X_* + (\mathbf{B}^T \mathbf{B} + \mathbf{R})^{-1} \mathbf{B}^T e_*, \quad (26)$$

where we introduced linear operators  $\mathbf{B}$  and  $\mathbf{R}$ . For an image  $U$ , these operators can be defined as  $\mathbf{B}U = B ** U$  and  $\mathbf{R}U = R ** U$ . If an image  $U$  is considered as a flat vector, the operators  $\mathbf{B}$  and  $\mathbf{R}$  correspond to square matrices of compatible size. Multiplying an image vector by such matrix yields the same result as a respective 2-D convolution;  $\mathbf{B}^T$  is a transposed matrix.

The inverse operator in (26) corresponds to inverting a very large matrix. The QP solver described in Section IV uses an iterative inversion method for a constrained version of the problem. (The unconstrained problem (25) is a special case). At each iteration, only forward computations are performed and the operators  $\mathbf{B}$  and  $\mathbf{R}$  are applied as FIR convolution operators.

The first term in (26) includes a recovery gain for the steady state signal  $X(t) = X_*$  and the second term contains the noise amplification gain. The design goal is to find an optimized tradeoff between the recovery gain  $(\mathbf{B}^T \mathbf{B} + \mathbf{R})^{-1} \mathbf{B}^T \mathbf{B}$  being close to unity (requires  $R$  to be small) and the noise amplification gain  $(\mathbf{B}^T \mathbf{B} + \mathbf{R})^{-1} \mathbf{B}^T$  being small (requires  $R$  to be large). This tradeoff is considered in more detail below.

#### B. Design of regularization operator

The convolution operator  $R$  can be conveniently designed in a spatial frequency domain; this is similar with established approaches to filter design. The frequency domain analysis and design is relative simple computationally and conceptually at the cost of neglecting the boundary effects.

To maintain the analysis rigor we embed the problem into a setup with modified boundary conditions. Most of the literature on MRF uses toroidal (circulant) boundary condition for frequency analysis. Another possibility is to consider an infinite lattice. Inside the image domain, away from the boundary, the two approaches are essentially equivalent.

This section considers the lattice to be infinite and uses a linear time-invariant spatially-invariant (LTSI) system model. The lattice is regular and the interactions between the neighbouring cells defined by the MRF potential (22)–(23) are identical for each cell up to the respective coordinate shift. More detailed justification of using LTSI models can be found in [1], [11] for distributed feedback systems and in [23] for multidimensional IIR filter design. A related but different filter design problem is considered in [21]. Boundary condition issues, which arise when the true system is not spatially infinite, can be integrated into the framework described herein as a deviation from the LTSI model, see [24], [39], [40].

We will use two-dimensional two-sided z-transform formulation for analysis in this section, see [47]. Let us denote by  $\lambda_1$  and  $\lambda_2$  the indeterminants corresponding to the two spatial indexes on the lattice. We will alternatively interpret  $\lambda_1$  and  $\lambda_2$  as complex variables in the 2-D two-sided z-transform or as unit index shift operators; this should be clear from the context.

The FIR regularization operator  $R$  in (24), (5) can be expressed through a 2-D transfer function

$$\hat{r}(\lambda_1, \lambda_2) = \sum_{-M \leq i, j \leq M} r_{ij} \lambda_1^i \lambda_2^j. \quad (27)$$

Similarly the FIR blur operator  $B$  in (7) can be expressed through a transfer function  $b(\lambda_1, \lambda_2)$ . Using the transfer function notation, (26) can be expressed as

$$x_e(\lambda_1, \lambda_2) = \frac{\hat{b}^\sim(\lambda_1, \lambda_2) \hat{b}(\lambda_1, \lambda_2)}{\hat{b}(\lambda_1, \lambda_2) \hat{b}^\sim(\lambda_1, \lambda_2) + \hat{r}(\lambda_1, \lambda_2)} x_*(\lambda_1, \lambda_2) + \frac{b^\sim(\lambda_1, \lambda_2)}{\hat{b}(\lambda_1, \lambda_2) \hat{b}^\sim(\lambda_1, \lambda_2) + \hat{r}(\lambda_1, \lambda_2)} e(\lambda_1, \lambda_2), \quad (28)$$

where  $\hat{b}^\sim(\lambda_1, \lambda_2) = \hat{b}(\lambda_1^{-1}, \lambda_2^{-1})$ .

The filter frequency responses can be obtained by considering the transfer functions in (28) on the unit circle, for  $\lambda_1 = e^{iv_1}$  and  $\lambda_2 = e^{iv_2}$  where  $v_1, v_2 \in [0, 2\pi]$  are real frequencies. The frequency responses of the operators  $R$  and  $B$  are

$$r(v_1, v_2) = \hat{r}(e^{iv_1}, e^{iv_2}), \quad b(v_1, v_2) = \hat{b}(e^{iv_1}, e^{iv_2}). \quad (29)$$

The design requirements are different in band and out-of-band. In-band frequency set is defined as  $\Omega_{In} \equiv \{(v_1, v_2) : b(v_1, v_2) > h_0\}$ , where  $h_0$  is a design parameter. In band the gain of the blur operator is sufficiently high and we can strive to invert it such that the signal is restored with a minimal

distortion. Out-of-band set is a complement of the in-band set. Out of band the blur operator gain is low and the noise overwhelms the signal. We give up the filter performance and specify limited noise amplification only. The in-band performance requires possibly small error of recovering the truth signal  $x_*$ . The first term gain in (26) should be close to unity inside the in-band frequency set  $\Omega_{In}$ .

$$\left| 1 - \frac{|b(v_1, v_2)|^2}{|b(v_1, v_2)|^2 + r(v_1, v_2)} \right| \leq s, \quad (v_1, v_2) \in \Omega_{In}, \quad (30)$$

where  $s$  is a performance parameter. (We further use  $s$  as a slack variable in the optimization).

The above filter performance objective should be combined with a requirement of noise amplification gain being limited (does not exceed an allowed value  $e_0$ ). This can be expressed as

$$\left| \frac{b(v_1, v_2)}{|b(v_1, v_2)|^2 + r(v_1, v_2)} \right| \leq e_0. \quad (31)$$

In this paper we assume that the blur operator  $B$  has central symmetry. Thus, the corresponding frequency response  $b(v_1, v_2) = \hat{b}(e^{iv_1}, e^{iv_2})$  is real for all frequencies. When designing the FIR regularization operator  $R$  we will look for a symmetric solution such that  $r(v_1, v_2)$  is real and positive.

For a symmetric  $R$  the real transfer function can be expanded as

$$\hat{r}(\lambda_1, \lambda_2) = \sum_{m=0}^{M_c} c_m P_m^M(\lambda_1, \lambda_2), \quad (32)$$

where  $P_m^M(\lambda_1, \lambda_2)$  are elementary polynomials defining the symmetry. The expansion (32) explicitly shows  $M_c + 1$  independent parameters  $c_m$  for the assumed symmetry type. We consider  $c_m$  to be decision parameters for the filter design. We assume an 8-fold symmetry:  $r_{m,n} = r_{-m,-n} = r_{-m,n} = r_{m,-n} = r_{n,m} = r_{-n,-m} = r_{-n,m} = r_{n,-m}$ . Then

$$\begin{aligned} P_0^M(\lambda_1, \lambda_2) &= 1, \\ P_j^M(\lambda_1, \lambda_2) &= \lambda_1^j + \lambda_1^{-j} + \lambda_2^j + \lambda_2^{-j}, \quad (j = 1, \dots, M) \\ P_{M+j}^M(\lambda_1, \lambda_2) &= \lambda_1^j \lambda_2^j + \lambda_1^{-j} \lambda_2^j + \lambda_1^j \lambda_2^{-j} + \lambda_1^{-j} \lambda_2^{-j}, \\ P_{2M+k}^M(\lambda_1, \lambda_2) &= \lambda_1^{l_k} \lambda_2^{m_k} + \lambda_1^{l_k} \lambda_2^{-m_k} + \lambda_1^{-l_k} \lambda_2^{m_k} \\ &+ \lambda_1^{-l_k} \lambda_2^{-m_k} + \lambda_1^{m_k} \lambda_2^{l_k} + \lambda_1^{m_k} \lambda_2^{-l_k} + \lambda_1^{-m_k} \lambda_2^{l_k} \\ &+ \lambda_1^{-m_k} \lambda_2^{-l_k}, \quad (l_k = 1, \dots, m_k - 1; m_k = 2, \dots, M), \end{aligned}$$

where the expansion size is  $M_c + 1 = 1 + 2M + M(M - 1)/2$ . The last equation gives a general case of the 8-fold symmetry and has  $k = 1, \dots, M(M - 1)/2$ , the second equation gives a special case of  $m_k = l_k$ , the first equation gives a special case of  $m_k = 0$  (or, the same,  $l_k = 0$ ).

The frequency response (32) can be expressed in the form

$$r(v_1, v_2) = \bar{P}^T(v_1, v_2)x, \quad (33)$$

$$x = [s \ c_0 \ c_1 \ \dots \ c_{M_c}]^T, \quad (34)$$

where  $x \in \Re^{M_c+2}$  is the decision vector including all the independent coefficients, i.e., our optimization variables and the additional decision variable - the slack variable  $s$  in (30). The regressor vector is

$$\bar{P}^T(v_1, v_2) = [0, P_1^M(e^{iv_1}, e^{iv_2}), \dots, P_{M_c+1}^M(e^{iv_1}, e^{iv_2})]$$

For each spatial frequency  $\nu$ , the frequency response  $r(v_1, v_2)$  is a linear function of the decision parameter vector  $x$ . Note that since  $r(v_1, v_2) \geq 0$ , the denominators in (31), (30) are real positive. By multiplying (31) and (30) through by the denominators and collecting all the terms we obtain the following constrained optimization problem

$$s \rightarrow \min, \quad (35)$$

$$\text{subject to } c(v_1, v_2) + D^T(v_1, v_2)x \geq 0, \quad (36)$$

where the vector  $c(v_1, v_2)$  and the matrix  $D^T(v_1, v_2)$  collect the linear inequalities expressing the problem (29), (31), (30), (34), (33).

The problem (35), (36) is convex. Similar to [24] one can introduce a grid of the frequency points and consider the inequality constraints (36) on the grid only. The problem then becomes a large linear program that can be efficiently solved by an off-the-shelf LP solver. The result of the solution is the optimal decision vector  $x$ , which defines the regularization operator  $R$  in accordance with (32), (34). The design of the regularization operator  $R$  needs to be carried out once, off-line, and provides a tuning for the proposed optimization-based filter. A specific example of the design is considered in Section V.

#### IV. A SPECIALIZED LARGE-SCALE QP SOLVER

This section describes an interior-point method for solving the problem (5)–(6). We follow the notation in Subsection III-A and with some overload of notation consider the images  $X(t)$  and  $Y(t)$  as flat vectors in  $\Re^{N_1 N_2}$  obtained by stacking all image elements.

The observation model (7) can be expressed as

$$Y(t) = \mathbf{B}x(t) + e(t),$$

where  $\mathbf{B} \in \Re^{N_1 N_2 \times N_1 N_2}$  is the blurring operator matrix corresponding to the convolution operator  $B$ . Similarly, we will consider the regularization operator matrix  $\mathbf{R} \in \Re^{N_1 N_2 \times N_1 N_2}$  corresponding to the convolution operator  $R$ .

The problem (5)–(6) can be written as

$$\begin{aligned} L = \frac{1}{2} \sum_{t=1}^{N_t} [\|Y(t) - \mathbf{B}X(t)\|^2 + X(t)^T \mathbf{R}X(t)] \\ + \frac{1}{\rho} \sum_{t=2}^{N_t} \|X(t) - X(t-1)\|_1 \rightarrow \min, \quad (37) \end{aligned}$$

subject to  $X(1) \geq 0$ ,  $X(t) \geq X(t-1)$ ,  $(t = 2, \dots, N_t)$ , (38)

where the inequality  $X(1) \geq 0$  is introduced without a loss of generality (we can always offset  $X(t)$  by  $\min_t Y(t)$ ). The problem (37)–(38) is a convex QP with the total number of variables  $M = N_1 N_2 N_t$ .

We introduce new variables

$$Z(1) = X(1), \quad Z(t) = X(t) - X(t-1), \quad t = 2, \dots, N_t.$$

In terms of these new variables, (37) is equivalent to finding  $Z(1), \dots, Z(N_t) \in \Re^{N_1 N_2}$  that solve

$$G(Z) \rightarrow \min \quad (39)$$

$$\text{subject to } Z(t) \geq 0, \quad t = 1, \dots, N_t, \quad (40)$$

where the decision vector is  $Z = (z(1), \dots, z(N_t)) \in \mathfrak{R}^{N_1 N_2} \times \dots \times \mathfrak{R}^{N_1 N_2}$  and the objective is

$$G(Z) = \frac{1}{2} \sum_{t=1}^{N_t} (\|Y(t) - \mathbf{B}[Z(1) + \dots + Z(t)]\|^2 + [Z(1) + \dots + Z(t)]^T \mathbf{R}[Z(1) + \dots + Z(t)]) + \frac{1}{\rho} \sum_{t=2}^{N_t} Z(t).$$

If  $Z^*(t) = (Z^*(1), \dots, Z^*(N_t))$  solves the problem (39)–(40), then

$$X^* = (X^*(1), \dots, X^*(N_t)) \in \mathfrak{R}^{N_1 N_2} \times \dots \times \mathfrak{R}^{N_1 N_2}$$

with  $X^*(t) = X(0) + \sum_{k=1}^t Z^*(k)$  solves the original problem (5)–(6).

#### A. The barrier method

The *logarithmic barrier* for the nonnegativity constraints  $Z(t) \geq 0$  in (39) is

$$\Phi(Z) = - \sum_{t=1}^{N_t} \sum_{i=1}^{N_1 N_2} \log Z_i(t), \quad (41)$$

with domain

$$\text{dom } \Phi = \{Z = (Z(1), \dots, Z(N_t)) \in \mathfrak{R}^{N_1 N_2} \times \dots \times \mathfrak{R}^{N_1 N_2} : Z_i(t) > 0, i = 1, \dots, M, t = 1, \dots, N_t\}.$$

The logarithmic barrier function (41) is smooth and convex in its domain.

We augment a weighted objective function of (39) by the logarithmic barrier (41), to obtain

$$\phi_\tau(Z) = \tau G(Z) + \Phi(Z), \quad (42)$$

where  $\tau > 0$  is a weighting parameter. This function is smooth, strictly convex, and bounded below, and so has a unique minimizer  $Z^*(\tau) \in \mathfrak{R}^M$ . The set  $\{Z^*(\tau) \mid \tau > 0\}$  defines a curve in  $\mathfrak{R}^M$ , parameterized by  $\tau$ , which is called the *central path*. In particular, the minimizer of (42) is no more than  $M/\tau$ -suboptimal, so the central path leads to an optimal solution. See [8, §11] for more on the central path and its properties.

In a classic primal barrier method, the barrier subproblem that finds the minimizer of (42) is solved for an increasing sequence of values of  $\tau$ . The Newton method for each subproblem is initialized at the optimal solution of the previous one. A typical method for increasing the parameter  $\tau$  is to multiply it by a factor on the order of 10 (see, e.g., [8, §10.3]). This is repeated until  $M/\tau$  is smaller than the required tolerance. Standard references on interior-point methods include [44], [45], [62], [63].

#### B. A truncated Newton interior-point method

We describe a method for solving the large-scale QP problem of the form (39)–(40). The method is the same as the barrier method except that the search direction is computed approximately, using a preconditioned conjugate gradients (PCG) method. When the search direction in Newton's method is computed approximately, using an iterative method such

as PCG, the overall algorithm is called a *conjugate gradient Newton method*, or a *truncated Newton method* [51], [12]. Truncated Newton methods have been applied within interior-point methods; see, e.g., [59], [48].

The search direction is computed as an approximation to the solution. The Newton system for the central path problem of minimizing (42) has the form

$$\mathbf{H} \Delta Z_{\text{nt}} = -g,$$

where  $\mathbf{H} = \nabla^2 \phi_\tau(Z) \in \mathfrak{R}^{M \times M}$  is the Hessian of the barrier objective and  $g = \nabla \phi_\tau(Z) \in \mathfrak{R}^M$  is the gradient. The Hessian  $\mathbf{H}$  is symmetric and positive definite matrix.

The PCG algorithm [13, §6.6] computes an approximate solution of the Newton system. It uses a preconditioner  $\mathbf{P}$ , a symmetric positive definite linear operator on  $\mathfrak{R}^{M \times M}$ . We will not go into the details of the PCG algorithm, and, instead, refer the reader to [31], [52], [45].

We use a simple preconditioner  $\mathbf{P}$  that approximates the Hessian of  $\tau G(z)$  with its diagonal entries, while retaining the Hessian of the logarithmic barrier:

$$\mathbf{P} = \tau \text{diag}(\nabla^2 G(Z)) + \nabla^2 \Phi(Z),$$

where  $I \in \mathfrak{R}^{M \times M}$  is an identity matrix,  $\eta$  is a parameter, and  $\text{diag}(S)$  is a diagonal matrix obtained by setting the off-diagonal entries of the matrix  $S$  to zero. The preconditioner is a diagonal matrix, since  $\nabla^2 \Phi(Z)$  is also a diagonal matrix,

$$\nabla^2 \Phi(Z) = \begin{bmatrix} \text{diag}(Z(1)) & & & \\ & \ddots & & \\ & & \ddots & \\ & & & \text{diag}(Z(N_t)) \end{bmatrix} \in \mathfrak{R}^{M \times M}.$$

Here  $\text{diag}(A)$  is the diagonal matrix whose diagonal entries are the entries of  $A$ .

The PCG algorithm needs a good initial search direction and an effective truncation rule.

*Initial point.* A good initial search direction requires on average fewer iterations of the PCG algorithm, and therefore can accelerate the method. There are many choices for the initial search direction, e.g., zero or the search direction found in the previous step of the method. The previous search direction appears to have a small advantage over the negative gradient and zero.

*Truncation rule.* The truncation rule for the PCG algorithm gives the condition for terminating the algorithm. Our implementation uses a simple truncation rule: the PCG algorithm stops when either the cumulative number of PCG steps exceeds the given limit  $N_{\text{pcg}}$ , or the gradient is less than the relative tolerance  $\epsilon_{\text{pcg}}$ . We change the relative tolerance adaptively as

$$\epsilon_{\text{pcg}} = \min \{0.1, \xi \eta / \|g\|_2\}, \quad (43)$$

where  $\eta$  is the duality gap at the current iteration and  $\xi$  is an algorithm parameter. The choice of  $\xi = 0.01$  appears to work well for a wide range of problems. In other words, we solve the Newton system with low accuracy at early iterations, and solve it more accurately as the duality gap decreases. Since the convergence of the PCG algorithm is usually very fast, there is no significant effect of  $N_{\text{pcg}}$  on the overall performance, as long as the limit is set to a large value.

Each iteration of the PCG algorithm involves a handful of inner products, the matrix-vector product  $\mathbf{H}p$  with  $p \in \mathbb{R}^M$  and a solve step with the preconditioner  $\mathbf{P}$  in computing  $\mathbf{P}^{-1}r$  with  $r \in \mathbb{R}^M$ . The solve step  $\mathbf{P}^{-1}r$  can be computed in  $O(M)$  flops, since  $\mathbf{P}$  is diagonal.

The most computationally expensive operation for a PCG step is the matrix-vector product  $\mathbf{H}p$  with  $p \in \mathbb{R}^M$ . The Hessian  $\mathbf{D} = \nabla^2 \Psi$  of the quadratic function

$$\Psi = \frac{1}{2} \sum_{t=1}^{N_t} \|Y(t) - \mathbf{B}X(t)\|^2 + X(t)^T \mathbf{R}X(t)$$

at  $X = (X(1), \dots, x(N_t))$  is the block diagonal matrix

$$\mathbf{D} = \text{block diag}(\mathbf{B}^T \mathbf{B} + \mathbf{R}^T \mathbf{R}, \dots, \mathbf{B}^T \mathbf{B} + \mathbf{R}^T \mathbf{R}) \in \mathbb{R}^{M \times M}.$$

Here we use  $\text{block diag}(A_1, \dots, A_p)$  to denote a matrix with diagonal blocks  $A_1, \dots, A_p$ . Using the chain rule of differentiation, we can see that the Hessian of the barrier objective  $\nabla^2 \phi_\tau$  at  $Z$  has the form

$$\mathbf{H} = \nabla^2 \Phi(Z) + \tau \mathbf{L}^T \text{block diag}(\mathbf{B}^T \mathbf{B} + \mathbf{R}^T \mathbf{R}, \dots, \mathbf{B}^T \mathbf{B} + \mathbf{R}^T \mathbf{R}) \mathbf{L}$$

where  $\mathbf{L}$  is the lower block-triangular matrix

$$\mathbf{L} = \begin{bmatrix} I & 0 & 0 & \dots & 0 \\ I & I & 0 & \dots & 0 \\ \vdots & \vdots & \vdots & \vdots & \vdots \\ I & I & I & \dots & I \end{bmatrix} \in \mathbb{R}^{M \times M}.$$

The product  $\mathbf{H}p$  can be computed as the following chain of operations:

$$\mathbf{H}p = \mathbf{L}^T u, \quad u = \mathbf{D}v, \quad v = \mathbf{L}p.$$

The vector  $v$  can be computed in  $O(M)$  flops, and  $u = \mathbf{D}v$  can be computed with  $N_t$  convolutions with the blurring and regularization filters. Finally, the vector  $\mathbf{L}^T u$  can be computed in  $O(M)$  flops. To sum up, the cost of computing  $\mathbf{H}p$  is  $O(M + N_t(N_b + N_r))$ , where  $N_b$  is the total cost of calculating the matrix vector products  $\mathbf{B}Z$  and  $\mathbf{B}^T Z$  with  $Z \in \mathbb{R}^M$ , and  $N_r$  is the cost of performing  $\mathbf{R}Z$  and  $\mathbf{R}^T Z$ . Those products can be computed efficiently using fast algorithms for two-dimensional convolution with the FIR kernels  $B$  and  $R$ . For  $\mathbf{B}$  and  $\mathbf{R}$  based on FIR convolution kernels, the products can be computed in  $O(M)$  flops.

Since the memory requirement of the truncated Newton interior-point method is modest, the method is able to solve very large problems, for which forming the Hessian  $\mathbf{H}$ , let alone computing the search direction, would be prohibitively expensive. The runtime of the truncated Newton interior-point method is determined by the product of  $s$ , the total number of PCG steps required over all iterations, and the cost of a PCG step. In extensive testing, we found that the total number of PCG steps ranges between a few hundred and several thousand to compute a solution with a relative tolerance of 0.01.

## V. APPLICATION TO STRUCTURAL HEALTH MONITORING

The proposed signal processing approaches were demonstrated for Structural Health Monitoring (SHM) data collected in laboratory experiments. The data collection conditions in the experiment were close to a real-life SHM operational environment.

### A. SHM sensing system

The experiments employed an SHM sensing system developed by Acellent Technologies. This system uses a network of distributed piezoelectric sensors/actuators embedded on a thin dielectric carrier film called the SMART Layer<sup>®</sup>, see [3], [4]. The SMART Layer technology has both active and passive sensing capabilities via the embedded piezoelectric transducers, see Figure 3. This sensor network is used with a portable diagnostic unit called the ScanGenie to query, monitor and evaluate the condition of a structure. In Active Sensing Mode, the ScanGenie in turn actuates each of the transducers to generate pre-selected diagnostic signals and transmit them to neighboring sensors. The responses can be interpreted in terms of damage size and location or material property changes. In Passive Sensing Mode the SMART Layer sensors can continuously monitor the structure for impact events. Both modes permit real-time structural analysis and evaluation along with constant collection of structural data and information while the structure/vehicle is in service. Specifically the system can:

- Obtain real-time, in-service, data on the integrity of an aircraft structure.
- Identify visible and invisible damage in metal and composite structures.
- Access damage data from structural anomalies including: i) fatigue cracks in highly loaded metallic fittings, ii) delaminations and disbonds in composite components, and iii) deterioration in bonded joints and iv) projectile impact damage.
- Reduce inspection and structural maintenance costs by providing an easy tool for maintenance personnel to assess damaged and take preventive action.

The SMART Layer can be as thin as 2 - 4 mil and as a result has little weight. Typical sensor sizes range from 0.125-0.25" in diameter with thickness of 0.01-0.03". The sensor network layers can be either surface mounted on both metallic and composite structure using an adhesive such as epoxy or embedded inside the composite structures during manufacturing by placing the sensor film between plies during lay-up.

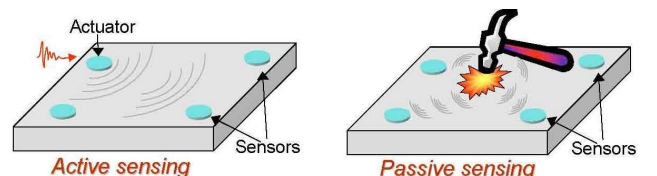


Fig. 3: SMART Layer technology has both active and passive sensing capabilities.

### B. Test data set

Current state-of-the-art damage detection methodologies rely on the use of baseline data collected from the structure in the undamaged state. The methodologies are based on comparing the current sensor responses to the previously recorded baseline sensor responses, and using the differences to glean information about structural damage. However, it is known that environmental effects, such as temperature differences, will also cause changes in the sensor signals. Thermal calibration techniques can be employed to mitigate the effect, but have limited accuracy, especially if the temperature falls outside of the calibrated range.

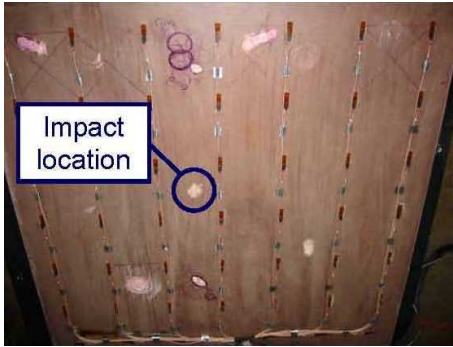


Fig. 4: Flat composite panel with 49 sensors.

In this study, impact tests were conducted on a 4' × 4' flat composite panel and collected sensor data at multiple temperatures. There were 49 sensors on the panel in a 7 × 7 grid with 7 inch spacing. The panel was impacted nine times in the same location to initiate and grow the damage, see Figure 4. Data was collected after each impact and the resulting diagnostic images were generated at two different temperatures: 20°C and 40°C. Thermal compensation was applied only over a small range of temperatures, from 25°C - 35°C, so the generated images fall outside the compensated range and therefore exhibit both damage and environmental variation. The images are illustrated in Figure 5.

To generate the images, a technique was employed that uses the Total Signal Energy (TSE) to calculate damage index values for each actuator-sensor path. The TSE of the scatter signal is compared to the TSE of the baseline signal and a corresponding damage index is calculated. The values for each path were used to generate a map highlighting the location of structural changes. The map was then smoothed using a two-dimensional finite impulse response filter to produce the final images. These images provide a visual representation of the location of structural changes and can be used as a qualitative measure of damage size.

The overall data set obtained in the experiments contains 8 pairs of images with  $171 \times 171 = 29,241$  pixels each. To demonstrate the proposed optimization filtering approach we used a Bootstrapping-like method to increase number of images in the sequence. From a single pair of the images  $\{Y_{20}(t), Y_{40}(t)\}$  obtained for the same panel damage at two different temperatures we create  $n_b > 2$  samples. We compute linear interpolations of the two images to approximate data for

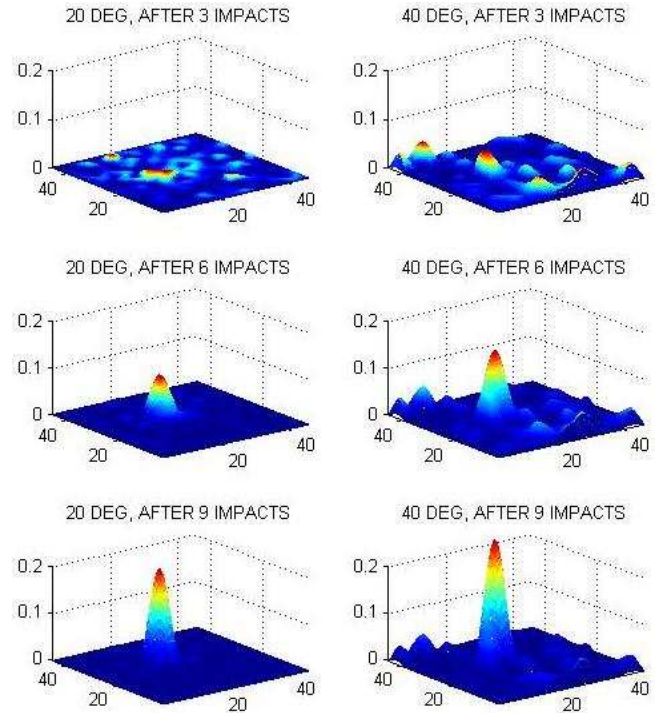


Fig. 5: Generated diagnostic images at 20°C and 40°C after 3, 6 and 9 impacts.

$n_b$  in-between temperatures

$$Y(\tau) = a_\tau Y_{20}(t) + (1 - a_\tau) Y_{40}(t), \quad (k = 1, \dots, n_b), \quad (44)$$

where  $\tau = n_b t + k$ , ( $k = 1, \dots, n_b$ ) is the time index of the generated data set and  $a_\tau$  are random variables uniformly distributed on the interval  $[0, 1]$ . We assumed  $n_b = 3$ : three scans were generated according to (44) for each damage state.

As Figure 5 illustrates, the environment variation is about 25% of the signal. For earlier scans, where less damage has yet accumulated, the signal/noise ratio is much worse than when estimating the damage from the diagnostic image data.

We assumed a Gaussian blur model with the half-width  $\sigma$  of 1.5 pixels. The PSF operator  $B$  is illustrated on the left plot in Figure 6. The noncausal FIR operator  $B$  used in the filtering algorithms had a maximal  $\pm 6$  pixels tap delay along each spatial coordinate. We did not identify the prior MRF model. Instead, we considered the model parameters as tuning factors in the filter design.

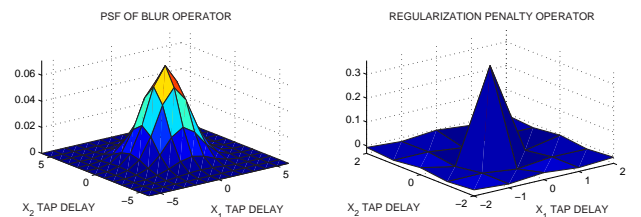
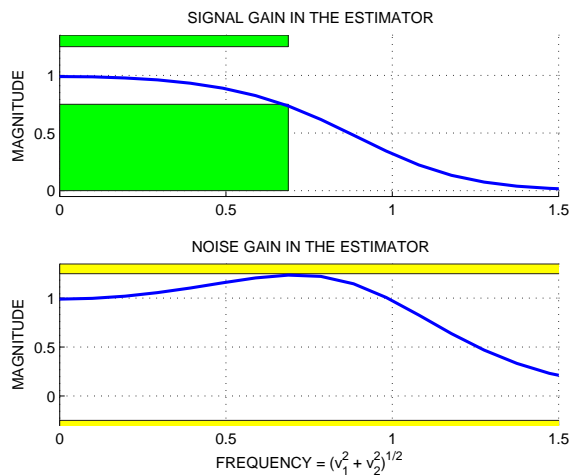


Fig. 6: Spatial operators in the optimization problem statement.

### C. Optimization-based filter design

The QP-optimization-based filtering problem (5)–(6) requires to define the FIR regularization operator  $R$  coming from the MRF prior model of the data. We designed the filter by considering  $R$  as a tuning knob and computing it as described in Section III.

By assuming a  $128 \times 128$  spatial frequency grid, the LP (35), (36) was solved to obtain a central symmetric operator  $R$  with  $M = 2$  tap delays. The in-band frequency set  $\Omega_{In}$  was chosen by considering a set of grid frequencies where the blur operator gain exceeds  $h_0 = 0.55$  of the maximal (zero-frequency) gain. The maximal noise amplification gain in (31) was chosen as  $e_0 = 1.25$ . The design yielded the in-band signal recovery distortion factor  $s = 0.2$  in (30).



**Fig. 7:** Frequency domain design of the regularization operator. The horizontal axis shows a magnitude of spatial frequency.

The frequency domain design is illustrated in Figure 7. The design is central symmetric and the 2-D transfer functions depend on the magnitude  $\sqrt{v_1^2 + v_2^2}$  of the spatial frequency vector. The upper plot in Figure 7 shows the estimator signal gain, the magnitude of the first term transfer function in (28). The lower plot shows the noise gain, the magnitude of the second term transfer function in (28).

The QP problem (5)–(6) and, thus, the filtering are fully described by two spatial FIR operators;  $B$  and  $R$ . Figure 6 illustrates the assumed blur operator and the designed penalty operator  $R$ . The two remaining scalar parameters in (5)–(6) were chosen as follows. The initial condition covariance parameter was assumed  $q_0 = 0$ . The time regularization penalty was assumed as  $\rho = 2$ .

### D. Filtering and trending results

The designed optimization-based filter was implemented using the solver discussed in Section IV. We solved the problem with relative accuracy 1%. The solver allows achieving much better relative accuracy, but this accuracy is more than adequate for any practical use. The algorithm was implemented in both Matlab and C, and run on a 3.2GHz Pentium IV under Linux. We use  $\eta = 1$  in the adaptive rule in (43).

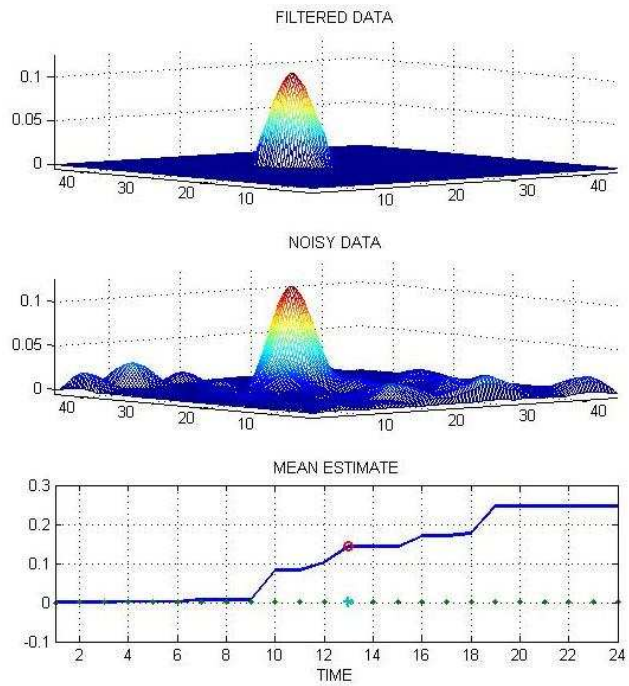


**Fig. 8:** Filtering results for the test data set.

The stopping criterion for the problem of minimization  $\phi_t$  is  $\|\nabla\phi_\tau(E)\|_F \leq 10^{-6}$ .

It was applied to the test data set illustrated in Figure 5. Because of the environmental variation, the raw images in Figure 5 show significant variation all over the image. By experiment design we know that in fact the damage is concentrated in a single spot.

The filtering results are shown in Figure 8. The displayed images are  $X(t) - X(1)$ . We assume that initially there is no damage and subtract the baseline. The upper plot in Figure 8 shows the last image of the filtered data  $X(24) - X(1)$ ; the middle plot shows the last image of the test data  $Y(24)$ . The upper plot in Figure 8 has a single peak which accurately recovers the damage location. The lower plot in Figure 8 displays the time evolution of the filtered signal averaged over an image patch of  $10 \times 10$  pixels around the damage peak (solid line). The dots show the time evolution of an average value outside of the patch. Both curves accurately reflect the available ground truth knowledge.

As one can see, the proposed nonlinear filtering scheme substantially improves the quality of the damage estimate. Though no ground truth data was available for the test set, the panel location where it was impacted and where the damage is likely concentrated is known. This is exactly what the filtered image shows. Because of the environmental variation, the raw images show phantom damage in multiple locations on the plate.

## VI. CONCLUSIONS

We have considered deblurring/denoising of a time series of images pixel-wise monotonic in time. The problem is motivated by structural health monitoring (SHM). The damage

accumulating in a structure needs to be distinguished from the data variation caused by changing environmental conditions.

We have formulated the problem as optimization of a log-likelihood index using a MRF model of the data. The proposed method for tuning the spatial regularization operator (MRF prior) sets the MRF weights based on specifications such as signal recovery performance and noise rejection.

Because of the monotonicity constraint, a large-scale structured QP problem needs to be solved numerically to obtain the estimate. The described interior-point method for solving large-scale QP problems of this type is implemented in Matlab and can handle quadratic programs with several million variables and constraints in a few ten minutes or so on a PC.

We have demonstrated an application of the approach to processing the diagnostic images of structural damage obtained in experiments with a thermal chamber. The varying specimen temperature shows as a noise affecting the damage data. An application of the proposed signal processing approach has allowed to recover the damage signal while completely eliminating the variation.

## VII. ACKNOWLEDGEMENTS

Dr. Bao Liu and Dr. Tom Chang from Acellent conducted the impact tests on the panel and collected the raw sensor data; the authors are grateful for their help and would like to recognize their contribution. The authors thank Kwangmo Koh, ISL, Stanford EE Department, for helpful comments and suggestions in the work on the large-scale sparse QP solver. The authors appreciate the contribution of Prof. Fu-Kuo Chang, Stanford AA Department, in initiating the interaction between the theoretical and experimental parts of this work.

## REFERENCES

- [1] B. Bamieh, F. Paganini, and M. Dahleh, "Distributed control of spatially-invariant systems," *IEEE Trans. on Automatic Contr.*, Vol. 47, No. 7, July 2002, pp. 1091–1107.
- [2] R. Barlow, D. Bartholomew, J. Bremner, and H. Brunk, *Statistical Inference under Order Restrictions; the Theory and Application of Isotonic Regression*, New York: Wiley, 1972.
- [3] S. Beard, A. Kumar, X. Qing, H. Chan, C. Zhang, and T. Ooi, "Practical issues in real-world implementation of Structural Health Monitoring systems," *Proc. SPIE on Smart Structures and Material Systems*, March 2005.
- [4] S. Beard, P. Qing, M. Hamilton, and D. Zhang, "Multifunctional software suite for Structural Health Monitoring using SMART technology," *Proc. 2nd European Workshop on Structural Health Monitoring*, July 2004, Germany.
- [5] J. Besag, "Spatial interaction and the statistical analysis of lattice systems (with discussion)," *Journ. of Royal Statistical Society, Series B*, Vol. 36, No. 2, 1974, pp. 192–326.
- [6] M. Best, and N. Chakravarti, "Active set algorithms for isotonic regression; a unifying framework," *Mathematical Programming*, Vol. 47, 1990, pp. 425–439.
- [7] A. Restrepo and A. Bovik, "Locally monotonic regression," *IEEE Trans. on Signal Processing*, Vol. 41, No. 9, 1993, pp. 2796–2810.
- [8] S. Boyd, and L. Vandenberg, *Convex Optimization*, Cambridge University Press, Cambridge, UK, 2004.
- [9] A. Buades, B. Coll, and J. Morel, "A review of image denoising algorithms, with a new one," *SIAM Journ. on Multiscale Modeling and Simulation*, Vol. 4, No. 2, 2005, pp. 490–530.
- [10] P. Combettes and V. Wajs, "Signal recovery by proximal forward-backward splitting," *SIAM Journal on Multiscale Modeling and Simulation*, Vol. 4, No. 4, 2005, pp. 1168–1200.
- [11] R. D'Andrea and G. Dullerud, "Distributed control for spatially interconnected systems," *IEEE Trans. on Automatic Control*, Vol. 48, No. 9, 2003, pp. 1478–1495.
- [12] R. Dembo and T. Steihaug, "Truncated-Newton algorithms for large-scale unconstrained optimization," *Mathematical Programming*, Vol. 26, 1983, pp. 190–212.
- [13] J. Demmel, *Applied Numerical Linear Algebra*. SIAM, 1997.
- [14] D. Dudgeon and R. Mersereau, *Multidimensional Digital Signal Processing*, Prentice-Hall, 1984.
- [15] M. Figueiredo and R. Nowak, "An EM algorithm for wavelet-based image restoration," *IEEE Transactions on Image Processing*, Vol. 12, No. 8, 2003, pp. 906–916.
- [16] H. Fu, M. Ng, M. Nikolova, and J. Barlow, "Efficient minimization methods of mixed  $\ell_1$ - $\ell_1$  and  $\ell_2$ - $\ell_1$  norms for image restoration," *SIAM Journ. on Scientific computing*, Vol. 27, No. 6, 2006, pp. 1881–1902.
- [17] D. Goldfarb and W. Yin, "Second-order cone programming based methods for total variation image restoration," *SIAM Journ. on Scientific Computing*, Vol. 27, No. 2, 2005, pp. 622–645.
- [18] R. Gonzalez and R. Woods, *Digital Image Processing*, 2nd ed., Upper Saddle River, N.J.: Prentice Hall, 2002.
- [19] G. Goodwin, M. Seron, and J. De Dona, *Constrained Control and Estimation*, Springer Verlag, 2004.
- [20] D. Gorinevsky, "Monotonic regression filters for trending gradual deterioration faults," *American Control Conference*, pp. 5394–5399, Boston, MA, June 2004.
- [21] D. Gorinevsky, "Feedback loop design and analysis for iterative localized image deblurring," *44th IEEE CDC and ECC'05*, Seville, Spain, December 2005.
- [22] D. Gorinevsky, "Optimal estimate of monotonic trend with sparse jumps," *American Control Conf.*, New York, NY, July 2007.
- [23] D. Gorinevsky and S. Boyd, "Optimization-based design and implementation of multi-dimensional zero-phase IIR filters," *IEEE Trans. on Circuits and Systems - I*, Vol. 53, No. 2, 2006, pp. 372–383.
- [24] D. Gorinevsky, S. Boyd, and G. Stein, "Design of low-bandwidth spatially distributed feedback," *IEEE Trans. on Automatic Control*, (accepted).
- [25] D. Gorinevsky and G. Gordon, "Spatio-temporal filter for structural health monitoring," *American Control Conf.*, Minneapolis, MN, June 2006.
- [26] D. Gorinevsky, G. Gordon, S. Beard, A. Kumar, and F.-K. Chang, "Design of integrated SHM system for commercial aircraft applications," *5th Internat. Workshop on Structural Health Monitoring*, Stanford, CA, September 2005.
- [27] D. Gorinevsky, S. Samar, J. Bain, and G. Aaseng, "Integrated diagnostics of rocket flight control," *IEEE Aerospace Conference*, Big Sky, MT, March 2005.
- [28] M. Hanke and J. Nagy, "Restoration of atmospherically blurred images by symmetric indefinite conjugate gradient techniques," *Inverse Problems*, Vol. 12, 1996, pp. 157–173.
- [29] L. He, M. Burger, and S. Osher, "Iterative total variation regularization with non-quadratic fidelity," *Journ. of Mathematical Imaging and Vision*, Vol. 26, No. 1–2, 2006, pp. 167–184.
- [30] D. Hochbaum, "An efficient algorithm for image segmentation, Markov random fields and related problems," *Journ. of the ACM*, Vol. 48, No. 4, 2001, pp. 686–701.
- [31] C. T. Kelley, *Iterative Methods for Linear and Nonlinear Equations*, vol. 16, *Frontiers in Applied Mathematics*. SIAM, Philadelphia, PA, 1995.
- [32] S.-J. Kim, K. Koh, M. Lustig, S. Boyd, and D. Gorinevsky, "A method for large-scale  $\ell_1$ -regularized least squares problems with applications in signal processing and statistics," *IEEE Journ. of Selected Topics in Signal Processing*, 2007. (submitted)
- [33] J. Lim, *Two-dimensional Signal and Image processing*, Englewood Cliffs, N.J.: Prentice Hall, 1990.
- [34] S. Li, *Markov Random Field Modelling in Computer Vision*, Springer-Verlag, 1995.
- [35] B. Hunt, "The application of constrained least squares estimation to image restoration by digital computer," *IEEE Trans. Computers*, Vol. C-22, No. 9, pp. 805–812, 1973.
- [36] S. Keerthi and D. DeCoste, "A modified finite Newton method for fast solution of large scale linear SVMs," *Journ. of Machine Learning Research*, Vol. 6, 2005, pp. 341–361.
- [37] K. Koh, S.-J. Kim, and S. Boyd, "An interior-point method for large-scale  $\ell_1$ -regularized logistic regression," Submitted to *Journ. of Machine Learning Research*, 2006.
- [38] V. Kolmogorov, *Primal-dual Algorithm for Convex Markov Random Fields*, 2005. Microsoft Technical Report MSR-TR-2005-117.
- [39] C. Langbort and R. D'Andrea, "Distributed control of spatially reversible interconnected systems with boundary conditions," *SIAM Journ. of Control and Optimization*, Vol. 44, No. 1, 2005, pp. 1–28.

- [40] S. Mijanovic, G. Stewart, G. Dumont, and M. Davies, "Design of an industrial distributed controller near spatial domain boundaries," *American Control Conference*, Vol. 4, pages 3574–3580, Boston, MA, June 30–July 3, 2004.
- [41] R. Molina, J. Mateos, and A. Katsaggelos, "Blind deconvolution using a variational approach to parameter, image, and blur estimation," *IEEE Tran. on Image Processing*, Vol. 15, No. 12, 2006, pp. 3715–3727.
- [42] MOSEK ApS, *The MOSEK Optimization Tools Version 2.5. User's Manual and Reference*, 2002. Available: [www.mosek.com](http://www.mosek.com).
- [43] J. Nagy, R. Plemmons, and T. Torgersen, "Iterative image restoration using approximate inverse preconditioning," *IEEE Tran. on Image Processing*, Vol. 5, No. 7, 1996, pp. 1151–1162.
- [44] Y. Nesterov and A. Nemirovsky, *Interior-Point Polynomial Methods in Convex Programming*, Volume 13 of *Studies in Applied Mathematics*. SIAM, Philadelphia, PA, 1994.
- [45] J. Nocedal and S. Wright, *Numerical Optimization*. Springer Series in Operations Research. Springer, 1999.
- [46] S. Osher, M. Burger, D. Goldfarb, J. Xu, and W. Yin, "An iterative regularization for method total variation based image restoration," *SIAM Journ. on Multiscale Modeling and Simulation*, Vol. 4, No. 2, 2005, pp. 460–489.
- [47] A. Oppenheim, R. Schaffer, and J. Buck, *Discrete-Time Signal Processing*, Prentice Hall, 1999.
- [48] L. Portugal, M. Resende, G. Veiga, and J. Júdice, "A truncated primal-infeasible dual-feasible network interior point method," *Networks*, Vol. 35, 2000, pp. 91–108.
- [49] A. Restrepo and A. Bovik, "On the statistical optimality of locally monotonic regression," *IEEE Trans. on Signal Processing*, Vol. 42, No. 6, 1994, pp. 1548–1550.
- [50] T. Robertson, F. Wright, and R. Dykstra, *Order Restricted Statistical Inference*, New York: Wiley, 1988.
- [51] A. Ruszczyński, *Nonlinear Optimization*. Princeton University Press, 2006.
- [52] Y. Saad, *Iterative Methods for Sparse Linear Systems*. SIAM, Philadelphia, 2nd edition, 2003.
- [53] S. Samar, D. Gorinevsky, and S. Boyd, "Moving horizon filter for monotonic trends," *IEEE Conf. on Decision and Control*, Paradise Island, Bahamas, December 2004.
- [54] S. Samar, D. Gorinevsky, and S. Boyd, "Embedded estimation of fault parameters in an unmanned aerial vehicle," *IEEE Conf. on Control Applications*, Munich, Germany, October 2006.
- [55] N. Sidiropoulos and R. Bro, "Mathematical programming algorithms for regression-based nonlinear filtering in  $R^N$ ," *IEEE Tran. on Signal Processing*, Vol. 47, No. 3, 1999, pp. 771–782.
- [56] *Structural Health Monitoring-The Demands and Challenges*, F.-K. Chang (Editor), CRC Press, Proc. 3rd Internat. Workshop on Structural Health Monitoring, Stanford, CA, September 2001.
- [57] *Structural Health Monitoring-From Diagnostics, Prognostics to Structural Health Management*, F.-K. Chang (Editor), Destech Publishing, Proc. 4th Internat. Workshop on Structural Health Monitoring, Stanford, CA, September 2003.
- [58] *Structural Health Monitoring-Advancements and Challenges for Implementation*, F.-K. Chang (Editor), Destech Publishing, Proc. 5th Internat. Workshop on Structural Health Monitoring, Stanford, CA, September 2005.
- [59] L. Vandenberghe and S. Boyd, "A primal-dual potential reduction method for problems involving matrix inequalities," *Mathematical Programming*, Vol. 69, 1995, pp. 205–236.
- [60] R. Vanderbei, *LOQO User's Manual — Version 3.10*, 1997. Available: <http://www.orfe.princeton.edu/loqo>.
- [61] C. Vogel and M. Oman, "Fast, robust total variation-based reconstruction of noisy, blurred images," *IEEE Trans. on Image Processing*, Vol. 7, No. 6, 1998, pp. 813–824.
- [62] S. Wright, *Primal-dual Interior-point Methods*. SIAM, Philadelphia, PA, USA, 1997.
- [63] Y. Ye, *Interior Point Algorithms: Theory and Analysis*. John Wiley & Sons, 1997.